Lattice instability at phase transitions near the Lifshitz point in proper monoclinic ferroelectrics

2006 J. Phys.: Condens. Matter 18 4047

(http://iopscience.iop.org/0953-8984/18/16/011)

INSTITUTE OF PHYSICS PUBLISHING JOURNAL OF PHYSICS: CONDENSED MATTER

J. Phys.: Condens. Matter **18** (2006) 4047–4064 doi:10.1088/0953-8984/18/16/011

Lattice instability at phase transitions near the Lifshitz point in proper monoclinic ferroelectrics

R M Yevych, Yu M Vysochanskii, M M Khoma and S I Perechinskii

Institute for Physics and Chemistry of Solid State, Uzhgorod National University, 88000 Uzhgorod, Ukraine

E-mail: vysochanskii@univ.uzhgorod.ua

Received 28 October 2005, in final form 27 February 2006
Published 7 April 2006
Online at stacks.iop.org/JPhysCM/18/4047

Abstract

The temperature dependence of acoustic properties of the $Sn_2P_2(Se_xS_{1-x})_6$ uniaxial ferroelectric in the vicinity of the Lifshitz point (LP) was investigated by Brillouin spectroscopy and analysed in the Landau–Khalatnikov approximation. An anomalous decrease of the longitudinal hypersound velocity in the paraelectric phase caused by fluctuation effects and crystal structure defects has been found near the LP. Besides this, a small softening of the transverse acoustic phonons is observed, which is due to their linear interaction with the soft optic mode found for incommensurate phase transitions in proper ferroelectrics. The lattice instability analysis of $Sn_2P_2S_6$ and $Sn_2P_2Se_6$ crystals and their solid solutions in a polarizable ion model shows that a possible reason for the absence of a soft acoustic mode is nonorthogonality of the spontaneous polarization vector and modulation wavevector which both lie in the monoclinic symmetry plane.

1. Introduction

The uniaxial proper ferroelectric solid solution $Sn_2P_2(Se_xS_{1-x})_6$ is special in that one may reach the vicinity of the Lifshitz point (LP) in the phase diagram, where paraelectric, ferroelectric and incommensurate phases meet. $Sn_2P_2S_6$ and $Sn_2P_2Se_6$ are isostructural monoclinic compounds with $P2_1/c$ symmetry in the high-temperature phase and Pc symmetry in the low-temperature phase [1, 2]. The phase sequence in $Sn_2P_2Se_6$ is similar to that in the well-known examples of thiourea [3] and $NaNO_2$ [4]: a phase transition (PT) of the second order from the paraelectric (PE) phase to the incommensurate (IC) phase at temperature T_i and a PT of the first order (lock-in transition) from the IC phase to the ferroelectric (FE) phase at temperature T_c, with a modulation wavevector in the IC phase near the Brillouin zone (BZ) centre [5]. In $Sn_2P_2S_6$ a direct second order PT from the PE phase to the FE phase is found at T_0. Because of the absence of the intermediate IC phase in the sulfur compound and its presence in the selenium compound, one expects a triple point in the temperature–concentration phase diagram for the $Sn_2P_2(Se_xS_{1-x})_6$ solid solution. Such a point, in which the $T_0(x)$ transition

line splits smoothly into $T_i(x)$ and $T_c(x)$ lines, was indeed observed, and identified as an LP, as was introduced for magnetic compounds earlier [7].

X-ray diffraction investigations [8] have shown that in $Sn_2P_2Se_6$ below T_i an IC phase appears with a modulation period of about 14 unit cells. Neutron scattering investigations [9] have confirmed that in the IC phase of the $Sn_2P_2Se_6$ crystal the modulus of the modulation wavevector is equal to $q_i \approx 0.09q_{max}$ and decreases to $q_i \approx 0.075q_{max}$ under cooling to T_c. Here q_{max} is the BZ boundary.

$Sn_2P_2S_6$ and $Sn_2P_2Se_6$ are uniaxial ferroelectrics; in the FE phase the spontaneous polarization vector lies in the symmetry plane, and varies in amplitude as well as in orientation as a function of temperature. The same happens for the wavevector modulation in the IC phase of $Sn_2P_2Se_6$. It also lies in the monoclinic plane of symmetry [8, 9]. The polarization wave in the IC phase may have a longitudinal component. If we choose the elementary cell as in [2], the [100] and [001] axes have approximately an angle of 91.16° between them, the spontaneous polarization vector in the symmetry plane makes an angle of approximately 15° with the [100] axis [10], and the modulation vector in the IC phase of $Sn_2P_2Se_6$ has an angle of approximately 9° with the [001] axis [8]. Thus, the modulation wave of $Sn_2P_2Se_6$ in its IC phase is close to a transverse wave, but it has a longitudinal component as well, which varies under temperature or chemical composition changes in the solid solutions.

In [11] a new universality class for the critical behaviour of the uniaxial ferroelectrics in the vicinity of the LP was found. The experimental data for $Sn_2P_2S_6$ concerning the anomalous behaviour of the dielectric susceptibility [12], ultrasound velocities [13], birefringence [14], and diffuse scattering of x-rays [15] are generally well described by [11] for the dipole Lifshitz point which is close to the tricritical point (TCP): the merging of these points preconditions a new universality class, the dipole tricritical Lifshitz point. However, the renormalization group description [11] is based on the uniaxial ferroelectric model of orthorhombic symmetry, when the modulation wave in its IC phase is exactly transverse. Therefore, the fluctuation spectrum of the order parameter is very interesting in the vicinity of LP for the uniaxial ferroelectrics with the polarization and modulation wavevector in the monoclinic symmetry plane.

The phenomenological description [16] assigns a major role to the Lifshitz type invariant for the appearance of the IC phase in proper ferroelectrics. In the thermodynamical potential this term represents a linear interaction of the soft optic and acoustic phonons, which is proportional to the distance from the BZ centre. The analysis of the phonon spectra of the $Sn_2P_2Se_6$ crystal obtained by inelastic neutron scattering [9] confirms this mechanism of the IC phase appearance in this crystal. In this situation one expects a decrease to zero of the transverse acoustic phonon velocity when approaching the LP in proper ferroelectrics, which is similar to the soft acoustic mode in the case of proper ferroelastics. According to data obtained from ultrasonic measurements [17] for $Sn_2P_2S_6$ there is only a partial softening of the transverse acoustic mode propagating along the [100] crystallographic direction and polarized along the [001] direction.

As it was noted, for monoclinic symmetry and with the spontaneous polarization vector and the modulation wavevector of the IC phase lying in the symmetry plane, the dipole–dipole interaction of the mixed soft optic and acoustic phonons might play a special role in the transition through the LP. The study of this is the purpose of the present paper. Its outline is as follows.

First we report on the investigation of hypersound velocity and attenuation temperature dependence of $Sn_2P_2(Se_xS_{1-x})_6$ crystals with $x = 0$, 0.15 and 0.28 performed by Brillouin spectroscopy. Then the data are analysed in the Landau–Khalatnikov (LK) model and interpreted by combining this with lattice dynamics calculations within the polarizable ion model of these crystals.

2. Elastic properties from Brillouin spectroscopy

2.1. Method

The Brillouin scattering spectra were studied using a He–Ne laser, and a pressure-scanned three-pass Fabry–Perot interferometer with an accuracy of 35 and free spectral range of 2.52 cm^{-1}. The right-angle scattering mode was used. The crystalline samples were placed in a UTREX cryostat in which the temperature was stabilized with an accuracy of 0.25 K. The spectra lines were fitted by Lorentzians.

The hypersound velocities V and attenuation α were calculated using the well-known formulae:

$$\Omega_0 = \frac{V}{c}\,\omega_0\sqrt{(n_0 - n_S)^2 + 4n_0 n_S \sin^2\frac{\theta}{2}};$$

$$\alpha = \frac{\delta\omega}{2V};$$

where Ω_0 is a Brillouin component shift, ω_0 is the frequency of the He–Ne laser, θ is the scattering angle, and n_0, n_S are indices of refraction for the stimulated and scattered light. The accuracy was about 3% for hypersound velocities and about 10% for attenuation determination.

Elastic moduli and velocity indicatrices were calculated on the basis of the experimental hypersound velocities by using the Christoffel relation

$$\left(\sum_{jk} c_{ijkl} n_j n_k - \rho v^2 \delta_{il}\right) p_l = 0$$

where c_{ijkl} are the elastic constants, n_i are the unit wavevector components, ρ is the density, v is the velocity and p_i are the unit polarization vector components.

In the calculations of the hypersound velocities the known refractive indices for the $Sn_2P_2S_6$ [18] were used, and it was assumed, for simplicity, that $n_0 = n_S = 3.0$. For $Sn_2P_2(Se_{0.28}S_{0.72})_6$ the main refractive indices were determined by the prism method: $n_0 = n_S = 3.25$; and for $Sn_2P_2(Se_{0.15}S_{0.85})_6$ by taking a linear approximation for the dependence of the refractive index on the concentration (we found $n_0 = n_S = 3.13$). In the calculations of the elastic modulus the experimental values of crystal density were used, which agree well with the theoretically determined values: $\rho_{Sn_2P_2S_6} \approx 3540$ kg m^{-3}, $\rho_{Sn_2P_2(Se_{0.28}S_{0.72})_6} \approx 4020$ kg m^{-3}.

The Brillouin scattering spectra determination was carried out on three different samples for each of the crystals under study. The frequency shifts and corresponding hypersound velocities for every one of the three acoustic phonons propagating in seven directions were determined from the spectra.

2.2. Experimental data

The part of experimental data mentioned below was reported previously without essential analysis [19]. Here we will try to remedy this situation. In figure 1, Brillouin scattering spectra of the $Sn_2P_2S_6$ and $Sn_2P_2(Se_{0.28}S_{0.72})_6$ crystals at room temperature are shown. The velocities obtained for $Sn_2P_2S_6$ are presented in table 1. The given quantities agree well with the data obtained by ultrasonic methods [13, 17] and with the data from inelastic neutron scattering experiments [20].

We have calculated the values of the c_{ij} elastic tensor components using the reciprocal Christoffel equations. These c_{ij} values are presented in table 1.

The hypersound velocities and elastic moduli for $Sn_2P_2(Se_{0.28}S_{0.72})_6$, in which the LP is found, are presented in table 2. Since the LP in $Sn_2P_2(Se_{0.28}S_{0.72})_6$ occurs at a temperature

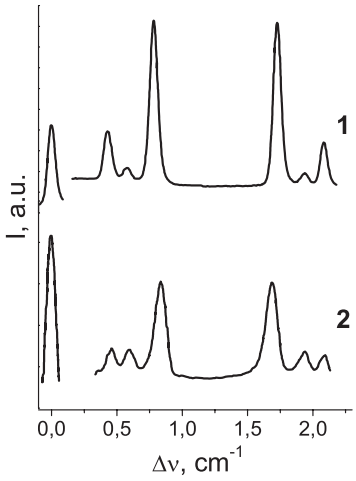

Figure 1. Brillouin spectra at $T = 293$ K. (1) For $Sn_2P_2S_6$ in the scattering geometry $Z(X\ X)Y$. (2) For $Sn_2P_2(Se_{0.28}S_{0.72})_6$ in the scattering geometry $Z(X\ 0)Y$.

Table 1. The magnitudes of sound velocities along different crystallographic directions (a) and elastic moduli (b) in the $Sn_2P_2S_6$ crystal at $T = 293$ K (elastic moduli obtained from the ultrasonic experiments are given in parentheses).

(a)

Direction	v_L, v_{T1}, v_{T2} (10^3 m s^{-1})
[100]	3.5, 2.5, 2.2
[010]	3.0, 2.4, 2.1
[001]	3.6, 2.4, 2.1
[110]	4.0, 2.3, 1.5
[011]	3.5, 2.5, 1.9
[101]	3.9, 2.4, 1.8
[10$\bar{1}$]	3.9, 2.4, 1.8

(b)

c_{ij} (10^{10} N m^{-2})					
4.2	2.0	1.8	0.0	−0.7	0.0
	3.2(3.25)	1.0	0.0	−0.4	0.0
		4.5(5.8)	0.0	0.5	0.0
			1.6	0.0	0.1
				2.2	0.0
					2.2

$T_{LP} \approx 286$ K, the magnitudes of hypersound velocities and elastic moduli, which are shown in table 2, correspond to elastic property anisotropy of the crystals under consideration in the PE phase at a temperature about $T_{LP} + 7$ K.

The Brillouin spectra as a function of temperature for phonons with $\vec{q} \parallel [010]$ in $Sn_2P_2S_6$ are shown in figure 2. The temperature dependence of the longitudinal hypersound velocity and attenuation obtained from these spectra are shown in figures 3 and 4. As can be seen from figure 4, there is a drastic change of the attenuation at the PT and a peak asymmetry towards the FE phase. This points to a relaxation mechanism of the attenuation, as is described by the LK model. At the same time the smearing of the anomaly in the hypersound velocity towards

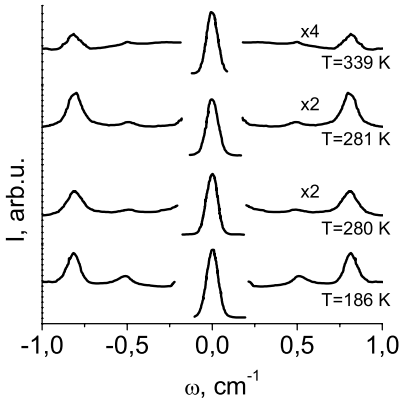

Figure 2. The Brillouin spectra temperature evolution for hypersound waves with $\vec{q} \parallel [010]$ in the $Sn_2P_2S_6$ crystal.

Table 2. The magnitudes of hypersound velocities along different crystallographic directions (a) and elastic moduli (b) in the $Sn_2P_2(Se_{0.28}S_{0.72})_6$ crystal at $T = 293$ K.

(a)						
Direction	v_L, v_{T1}, v_{T2} (10^3 m s^{-1})					
[110]	3.6, 2.3, 1.6					
[011]	3.4, 2.4, 1.8					
[101]	3.6, —, 1.7					
[10$\bar{1}$]	3.5, —, 1.7					
[111]	3.5, 2.4, 1.7					
[11$\bar{1}$]	3.5, 2.3, 1.9					
(b)						
c_{ij} (10^{10} N m^{-2})						
5.3	0.6	2.0	0.0	1.3	0.0	
	4.4	1.0	0.0	0.0	0.0	
		5.2	0.0	−1.2	0.0	
			1.8	0.0	0.3	
				1.3	0.0	
					2.1	

the PE phase shows the influence of order parameter fluctuations as well as crystal structure defects on the temperature dependence of acoustic properties of the crystal in the vicinity of the PT.

Figure 5 shows the temperature dependence of the longitudinal hypersound velocity with $\vec{q} \parallel [001]$. This dependence is similar to the behaviour of a longitudinal wave with $\vec{q} \parallel [010]$. However, for the hypersound velocity propagating along the [001] direction in the symmetry plane, the jump at the PT is smaller than that of the hypersound wave propagating along the [010] direction. There is a much smaller peak in the temperature dependence of the attenuation too (see figure 6). The spontaneous polarization vector is oriented in the symmetry plane close to the [100] direction. Since in the monoclinic $Sn_2P_2S_6$ the spontaneous polarization vector can have some component along the [001] direction the macroscopic field probably suppresses slightly the relaxation anomaly of the hypersound velocity and attenuation in the [001] direction.

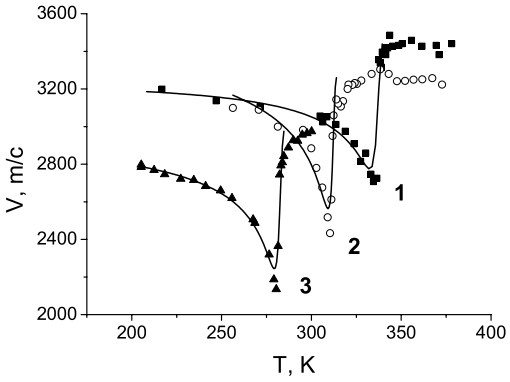

Figure 3. The temperature dependence of the longitudinal hypersound velocity with $\vec{q} \parallel [010]$. (1) $Sn_2P_2S_6$, (2) $Sn_2P_2(Se_{0.15}S_{0.85})_6$ and (3) $Sn_2P_2(Se_{0.28}S_{0.72})_6$. Solid lines: calculation according to relation (10).

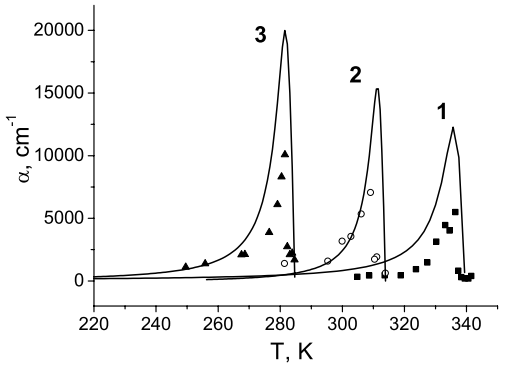

Figure 4. The temperature dependence of the longitudinal hypersound attenuation with $\vec{q} \parallel [010]$. (1) $Sn_2P_2S_6$, (2) $Sn_2P_2(Se_{0.15}S_{0.85})_6$, (3) $Sn_2P_2(Se_{0.28}S_{0.72})_6$. Solid lines: calculation according to relation (8).

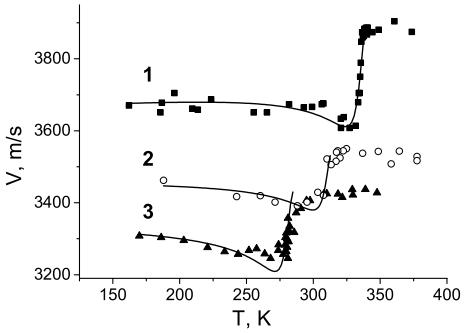

Figure 5. The temperature dependence of the longitudinal hypersound velocity with $\vec{q} \parallel [001]$. (1) $Sn_2P_2S_6$, (2) $Sn_2P_2(Se_{0.15}S_{0.85})_6$, (3) $Sn_2P_2(Se_{0.28}S_{0.72})_6$. Solid lines: calculation according to relation (13).

The spontaneous polarization macroscopic field influence is clearly seen for the [100] direction. Figure 7 shows the temperature dependence of the longitudinal hypersound velocity with $\vec{q} \parallel [100]$. A clear broadening of the spectral lines for the corresponding Brillouin component at the PT could not be observed. Therefore, the anomalous hypersound attenuation could not be detected within the experimental accuracy. As we can see, there is a small jump in the temperature dependence of the hypersound velocity. From the comparison with the ultrasonic data [17] it follows that the ultrasound velocity jump decreases with increasing ultrasound wave frequency: from 500 to 200 m s^{-1} in a frequency range 10–70 MHz, to 100 m s^{-1} at frequency about 10 GHz (our data). This behaviour can be explained in the following way. For the ultrasonic wave, which has a length of about 50 μm, the existence of the domain structure in the FE phase is very important. An estimation of the domain size in

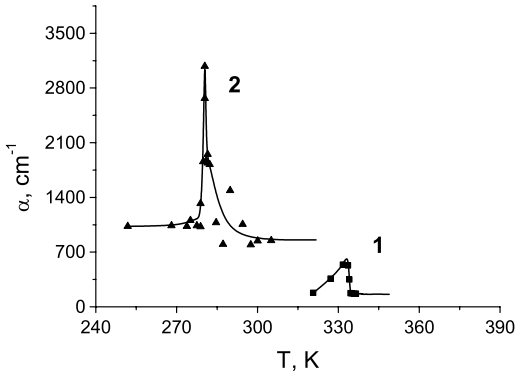

Figure 6. The temperature dependence of the longitudinal hypersound attenuation with $\vec{q} \parallel [001]$. (1) $Sn_2P_2S_6$, (2) $Sn_2P_2(Se_{0.28}S_{0.72})_6$. The solid lines are guides for the eyes.

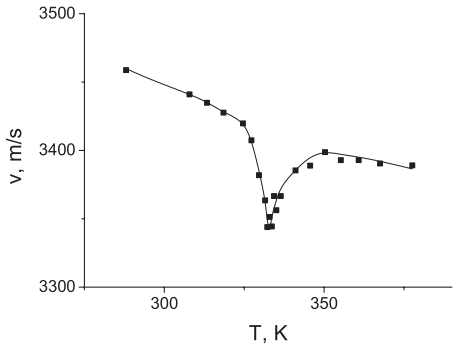

Figure 7. The temperature dependence of the longitudinal hypersound velocity with $\vec{q} \parallel [100]$ in the $Sn_2P_2S_6$ crystal.

$Sn_2P_2S_6$ was made earlier [21]: it gives values of its linear dimension in the range 20–60 μm. Hence there is a variation in the ratio of the domain size and the sound wavelength when the sound frequency changes, which determines the velocity dispersion along the direction of spontaneous polarization in the FE phase. For the hypersound waves whose length is three orders smaller than that for the ultrasonic ones, the macroscopic field in a polar direction suppresses relaxation anomalies in the temperature dependences of velocity and attenuation.

In the concentration phase diagram of the $Sn_2P_2(Se_xS_{1-x})_6$ solid solution, the LP is situated at $x_L \approx 0.28$, $T_L \approx 286$ K. To study the interaction between the soft optic mode and acoustic phonons when approaching the LP, temperature measurements of hypersound velocities and attenuation along different crystallographic directions for $Sn_2P_2(Se_{0.15}S_{0.85})_6$ and $Sn_2P_2(Se_{0.28}S_{0.72})_6$ were carried out. Figures 3 and 4 show the temperature dependence of the hypersound velocity and attenuation with propagation direction [010] for $Sn_2P_2(Se_{0.15}S_{0.85})_6$ and $Sn_2P_2(Se_{0.28}S_{0.72})_6$. When the selenium content is increased, the hypersound velocity in the PE phase decreases, and has a jump at the PT: $\Delta v_{22}(x = 0) \approx 760$ m s^{-1}, $\Delta v_{22}(x = 0.15) \approx 840$ m s^{-1}, $\Delta v_{22}(x = 0.28) \approx 920$ m s^{-1}. Such an increase of the hypersound velocity jump is expected for an approach to the LP and TCP. At the same time, while approaching the LP, the hypersound velocity anomaly tails towards the PE phase are rising. The maximum of the hypersound attenuation peak in the region of the PT grows as the selenium concentration increases.

When one approaches the LP, the jump in $v_{33}(T)$ at the PT decreases (see figure 5), and the spreading of this jump increases towards the PE phase. Significant changes are found in the temperature dependence of attenuation. As can be seen from figure 6, the attenuation peak has a 'tail' towards the PE phase for the $Sn_2P_2(Se_{0.28}S_{0.72})_6$ composition. This phenomenon

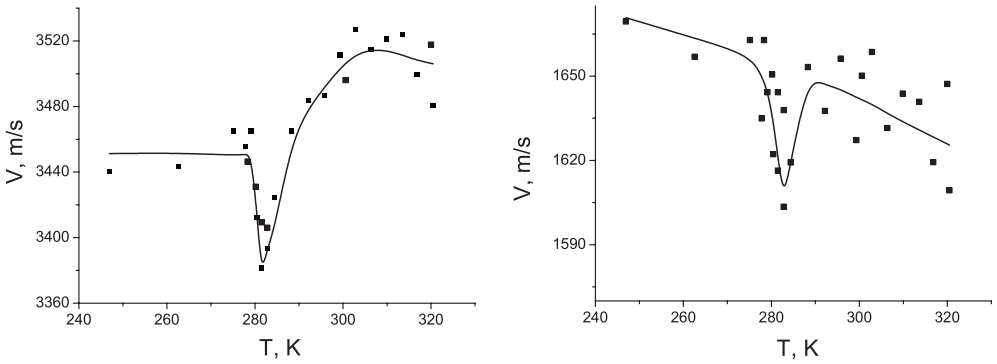

Figure 8. The temperature dependence of longitudinal (left) and transverse (right) sound velocities with $\vec{q} \parallel [101]$ in $Sn_2P_2(Se_{0.28}S_{0.72})_6$.

is connected to the increase of the order parameter fluctuations, as well as to the more intense spreading of critical anomalies by crystal structure defects when one approaches the LP. These two contributions were observed and analysed earlier [14] for $Sn_2P_2(Se_xS_{1-x})_6$ on the basis of birefringent investigations.

For $Sn_2P_2(Se_{0.28}S_{0.72})_6$, the temperature dependence of the velocity for the longitudinal and transverse hypersound propagating along the [101] direction was also investigated (see figure 8). This dependence has a minimum in the vicinity of the PT. This minimum stems from the linear interaction between the soft optic and acoustic phonons near the BZ centre. For directions in the symmetry plane the linear interaction with the longitudinal as well as the transverse acoustic phonons is allowed for the soft optic phonons.

2.3. Phenomenological analysis

Using the Landau theory of second order PT, one can describe the sound velocity and attenuation anomalies. For the case of a one-component ($\vec{P} = (P, 0, 0)$) order parameter and strain interaction the thermodynamical potential can be written [22] in the following form:

$$\Phi = \Phi_0 + \tfrac{1}{2}\alpha P^2 + \tfrac{1}{4}\beta P^4 + \tfrac{1}{6}\gamma P^6 + c_{ij}u_i u_j + q_{11i}u_i P^2 + r_{11ij}u_i u_j P^2 + \ldots, \tag{1}$$

where α, β, γ are expansion coefficients, $\alpha = \alpha_T(T - T_0)$, and the temperature dependence of the other coefficients is neglected; c_{ij} are elastic moduli; q_{ijk}, and r_{ijkl} are linear and quadratic electrostriction coefficients, respectively. From the expression (1) and the minimum condition $\partial\Phi/\partial P = 0$ one obtains for the polarization equilibrium value in the FE phase, under the absence of strain,

$$P_0^2 = \frac{\beta}{2\gamma}\left[\sqrt{1 - \frac{4\gamma\alpha_T}{\beta^2}(T - T_0)} - 1\right]. \tag{2}$$

The kinetic equation which describes the velocity of the polarization P approaching its equilibrium value P_0 has the form

$$\frac{\partial P}{\partial t} = -\frac{1}{L}\frac{\partial\Phi}{\partial P}, \tag{3}$$

where L is a kinetic coefficient with a slight temperature dependence. Expanding the $\partial\Phi/\partial P$ derivative in a power series in the difference $P - P_0$ we get

$$\frac{\partial P}{\partial t} = -\frac{1}{\tau}(P - P_0), \tag{4}$$

where $\tau = \chi L$ is the relaxation time, and $\chi = (\partial^2\Phi/\partial P^2)^{-1}$ is the dielectric susceptibility. Solving the given equation and taking into account (2), we obtain the following expression for the jump in the complex elastic modulus at the PT [23]:

$$\Delta c^*_{ijkl} = -\frac{1}{1+\mathrm{i}\omega\tau}\cdot\frac{\partial^2\Phi}{\partial P\partial u_{ij}}\left(\frac{\partial^2\Phi}{\partial P^2}\right)\frac{\partial^2\Phi}{\partial P\partial u_{kl}}, \tag{5}$$

or

$$\Delta c^*_{ij} = -\frac{1}{1+\mathrm{i}\omega\tau}\left[\frac{2q_{1i}q_{1j}}{\beta\sqrt{1-\frac{4\alpha\gamma}{\beta^2}}} + \frac{r_{1ij}\beta}{2\gamma}\left(\sqrt{1-\frac{4\alpha\gamma}{\beta^2}}-1\right)\right]. \tag{6}$$

The coefficient α and the relaxation time τ in expression (6) depend on temperature. Since $\tau = \chi L$ we can set $\tau = \tau_0/(T-T_0)$. The real part of the complex elastic modulus is connected with the sound velocity, and the imaginary part with the attenuation. Taking into account that $\Delta c = \rho(v^2 - v^2_\infty)$, where the value v_∞ is equal to the sound velocity in the PE phase, we obtain the temperature dependence of velocity and attenuation from (6):

$$v^2_{ij} = v^2_{ij\infty} - \frac{1}{1+\omega^2\tau^2}\left[\frac{2q_{1i}q_{1j}}{\rho\beta\sqrt{1-\frac{4\alpha\gamma}{\beta^2}}} + \frac{r_{1ij}\beta}{2\gamma\rho}\left(\sqrt{1-\frac{4\alpha\gamma}{\beta^2}}-1\right)\right], \tag{7}$$

$$\alpha = \frac{v^2_\infty - v^2}{2v^3}\omega^2\tau. \tag{8}$$

It should be noted that the sound wave frequency ω is not a constant in Brillouin scattering investigations as it is in the case of ultrasonic measurements. Therefore equation (7), in fact, is a biquadratic equation in v.

To analyse the temperature dependence of the longitudinal sound velocity with $\vec{q} \parallel [010]$ (see figure 3), we express this by means of c_{ij} coefficients. Let us solve the Christoffel equation for the given values of $\vec{q}$ and $\{c_{ij}\}$. We obtain

$$\rho v^2_{22} = c_{22}; \qquad (c_{66} - \rho v^2_i)(c_{44} - \rho v^2_i) = c^2_{46}, \tag{9}$$

where $v_i = v_{21}, v_{23}$ (the first index denotes the wave propagating direction, the second one the polarization). In other words, the pure longitudinal wave propagates in this direction, and its velocity is expressed through only one c_{22} coefficient (polarization vector (010) corresponds to the eigenvalue v_{22}). Taking into account that $\Delta c = \rho(v^2 - v^2_\infty)$, we obtain the temperature dependence of v_{22}:

$$v^2_{22} = v^2_{22\infty} - \frac{1}{1+\omega^2\tau^2}\left[\frac{2q^2_{12}}{\rho\beta\sqrt{1-\frac{4\alpha\gamma}{\beta^2}}} + \frac{r_{122}\beta}{2\gamma\rho}\left(\sqrt{1-\frac{4\alpha\gamma}{\beta^2}}-1\right)\right]. \tag{10}$$

In expression (10) the $v_{22\infty}$ value is equal to the equilibrium sound velocity in the PE phase. In our case $v_{22\infty} = 3440\ \mathrm{m\,s^{-1}}$. We take the estimation of the thermodynamical potential parameters we carried out earlier [6], and use them for an estimate of the linear and quadratic electrostriction coefficients. Thus, according to [6], for $Sn_2P_2S_6$ the expansion coefficients are equal to $\alpha_T = 1.6\times10^6\ \mathrm{J\,m\,C^{-2}\,K^{-1}}$, $\beta = 7.4\times10^8\ \mathrm{J\,m^5\,C^{-4}}$, and $\gamma = 3.5\times10^{10}\ \mathrm{J\,m^9\,C^{-6}}$. The result of fitting the experimental data by (10) is shown in figure 3. The best agreement of the theoretical curve with the experimental data is achieved for the parameter values $q_{12} = 3.6\times10^9\ \mathrm{J\,m\,C^{-2}}$, $r_{122} \approx 0$, and $\tau_0 = 2.8\times10^{-11}$c. It should be noted that the obtained value for q_{12} agrees well with the value $q_{12} = 4\times10^9\ \mathrm{J\,m\,C^{-2}}$ in [24].

Considering the hypersound waves along the [100] and [001] crystallographic directions, we notice that for the monoclinic crystal the longitudinal wave is quasi-longitudinal. There is,

however, one pure transverse wave with the polarization vector along the [010] axis. Solving the Christoffel equation for the mentioned directions of sound propagation, one obtains, similarly to (9), the following expressions for the velocities:

$$\begin{array}{lll} \vec{q} \parallel [100] : \rho v_{12}^2 = c_{66}; & (c_{11} - \rho v_i^2)(c_{55} - \rho v_i^2) = c_{15}^2, & v_i = v_{11}, v_{13}; \\ \vec{q} \parallel [001] : \rho v_{32}^2 = c_{44}; & (c_{33} - \rho v_i^2)(c_{55} - \rho v_i^2) = c_{35}^2, & v_i = v_{31}, v_{33}. \end{array} \tag{11}$$

By taking into account that the monoclinic angle in the $Sn_2P_2S_6$ crystals is close to a right angle, the c_{15} and c_{35} coefficients in (11) can be neglected (for rhombohedral symmetry they are equal to zero). As can be seen from table 1, the absolute values of these coefficients are small compared to c_{11}, c_{33} and c_{55}. Therefore, from (11) in the given approximation we obtain $\rho v_{11}^2 \approx c_{11}$, $\rho v_{33}^2 \approx c_{33}$, and from (6),

$$v_{11}^2 = v_{11\infty}^2 - \frac{1}{1+\omega^2\tau^2}\left[\frac{2q_{11}^2}{\rho\beta\sqrt{1-\frac{4\alpha_T\gamma}{\beta^2}}} + \frac{r_{111}\beta}{2\gamma\rho}\left(\sqrt{1-\frac{4\alpha_T\gamma}{\beta^2}} - 1\right)\right]. \tag{12}$$

$$v_{33}^2 = v_{33\infty}^2 - \frac{1}{1+\omega^2\tau^2}\left[\frac{2q_{13}^2}{\rho\beta\sqrt{1-\frac{4\alpha_T\gamma}{\beta^2}}} + \frac{r_{133}\beta}{2\gamma\rho}\left(\sqrt{1-\frac{4\alpha_T\gamma}{\beta^2}} - 1\right)\right]. \tag{13}$$

The analysis of the temperature dependence of the sound velocity propagating along the [001] direction in $Sn_2P_2S_6$ (see figure 5) in the framework of the LK model shows that the term responsible for the quadratic electrostriction plays an important role. Describing by equation (13) the experimental dependence (figure 5), the q_{13} and r_{133} coefficient values were obtained as 2.8×10^9 J m C^{-2} and 4.0×10^{10} N m^2 C^{-2}, respectively, at $\tau_0 = 4.6 \times 10^{-11}c$ ($q_{13} = 3.3 \times 10^9$ J m C^{-2} from previous work [24]).

Let us analyse the anomalies in the temperature dependence of the sound velocity along the [010] direction in $Sn_2P_2(Se_xS_{1-x})_6$ (see figure 3). They are an indication for a behaviour according to the LK model. For the analysis within this model according to equation (10), we use for the solid solution the known [6] α, β and γ coefficients of the thermodynamical potential (1). Then we may describe the sound velocity anomalies with the following electrostriction coefficients: for $Sn_2P_2(Se_{0.15}S_{0.85})_6$: $q_{12} = 3.5 \times 10^9$ J m C^{-2}, $r_{122} = 10 \times 10^{10}$ N m^2 C^{-2}; for $Sn_2P_2(Se_{0.28}S_{0.72})_6$: $q_{12} = 3.4 \times 10^9$ J m C^{-2}, $r_{122} = 2 \times 10^{10}$ N m^2 C^{-2}. Comparing these values with the analogous ones for $Sn_2P_2S_6$ shows a weak dependence on concentration within the experimental inaccuracy.

The analysis of the temperature anomalies of the hypersound velocity along [001] (see figure 5) in accordance to (13) gives the following values for the parameters: $Sn_2P_2(Se_{0.15}S_{0.85})_6$: $q_{13} = 2.2\times10^9$ J m C^{-2}, $r_{133} = 1.1\times10^{10}$ N m^2 C^{-2}; $Sn_2P_2(Se_{0.28}S_{0.72})_6$: $q_{13} = 2.6 \times 10^9$ J m C^{-2}, $r_{133} = 0.9 \times 10^{10}$ N m^2 C^{-2}.

2.4. Orientation dependence

To get a better view of the crystal lattice instability in the PE phase of $Sn_2P_2(Se_xS_{1-x})_6$, the direction dependence of the hypersound velocity was investigated. The longitudinal and transverse hypersound velocities were determined by Brillouin scattering methods for a number of propagation directions and at several temperatures. Using these sound velocities, the elastic tensor was determined. With these elastic tensor elements, the sound velocities of longitudinal and transverse waves may be determined for any direction in the crystal. The characteristic surfaces, which illustrate the anisotropy of the elastic properties, were then calculated. We shall discuss the cut of these surfaces by the main crystallographic planes.

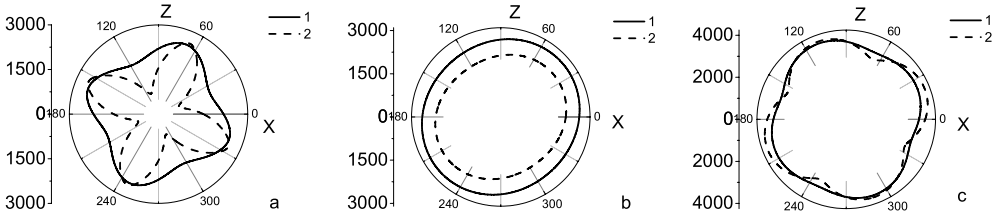

Figure 9. Velocity indicatrices of acoustic phonons propagating in the symmetry plane (010): (1) in the PE phase of $Sn_2P_2S_6$ (340 K), and (2) for $Sn_2P_2(Se_{0.28}S_{0.72})_6$ in the PE phase (293 K). (a) transverse phonons polarized in the symmetry plane (010); (b) transverse phonons polarized in the [010] direction; (c) longitudinal phonons polarized in the (010) symmetry plane.

The elastic matrices at room temperature for $Sn_2P_2S_6$ and $Sn_2P_2(Se_{0.28}S_{0.72})_6$, corresponding to the FE and the PE phases of these crystals, respectively, were given above (see tables 1 and 2). To compare the data in the PE phase the temperature behaviour of the elastic moduli and the orientation dependence of the sound velocities were determined for $Sn_2P_2S_6$.

The calculated orientation dependence of velocities of the longitudinal and two transverse waves with propagation direction lying in the symmetry plane are shown in figure 9. Comparing these dependences for $Sn_2P_2S_6$ and $Sn_2P_2(Se_{0.28}S_{0.72})_6$ in the PE phase near the PT temperature, it is possible to conclude that some softening occurs of the quasi-transverse acoustic phonons, which are polarized and propagate in the (010) plane and are connected by the elastic strain u_{xz}, when approaching the LP.

Let us examine the origin of the lattice instability for the $Sn_2P_2(Se_xS_{1-x})_6$ proper ferroelectrics. The interaction of the order parameter fluctuations with the elastic degrees of freedom plays an essential role in the mechanism of the PT to the IC phase in proper ferroelectrics. A shift of the dispersion branches minimum of the interacting soft optic and acoustic phonons from the BZ centre is connected with the increasing of this interaction. In the case of $Sn_2P_2S_6$-like crystals the linear interaction between the soft TO mode and the transverse acoustic TA mode along q_y, and polarized along the X axis, is involved. This interaction is proportional to the wavevector modulus and both modes attain a similar B symmetry at $q_y \neq 0$. Moving away from the BZ centre along q_z, the soft TO mode and mixed quasi-longitudinal and quasi-transverse acoustic vibrations polarized in the XZ plane attain the same A′ symmetry which allows the linear interaction. These situations are characterized by the occurrence of $(\partial\eta/\partial Y) \cdot u_{xy}$-like or $(\partial\eta/\partial Z) \cdot u_{xz}$-like gradient invariants of the Lifshitz type (where η is an order parameter). Thus, the wavevector of the IC phase and its temperature range, which are defined by a form of a dispersion branch of the interacting soft optic and acoustic phonons, depend considerably on the elastic moduli. If the dispersion surface of the soft optical mode is close to the isotropic one, the direction characterized by the smallest velocity of the transverse elastic wave is the most favourable for the production of the modulation vector of the IC phase.

Note that in $Sn_2P_2S_6$-like crystals the TO mode along q_y interacts linearly only with the lower TA branch, whereas the interaction with the LA branch occurs along q_z too and this branch may serve as a mediator which produces a linear coupling between the soft TO and TA phonons. Moreover, due to a full-symmetric character of the u_{xz} shift, there is an $\eta^2 u_{xz}$ invariant. A term $\eta^2 u_{xy}$ is forbidden by symmetry, and thus, for transverse acoustic phonons, propagating along the Z axis, the nonlinear interaction with the order parameter fluctuations is allowed in the lowest order (for longitudinal phonons this holds for $\eta^2 u_{ii}$). Due to the increase of the fluctuations when the PT is approached from the PE phase, this promotes the reduction of the velocity of TA phonons with q_z. The fluctuation variation of the velocity of

TA phonons with q_y must be much less since only a biquadratic nonlinear coupling of $\eta^2 u_{xy}^2$ is allowed. These facts agree qualitatively with the softening of quasi-transverse acoustic phonons polarized in the (010) plane and propagating near the direction of the modulation wavevector in the IC phase of $Sn_2P_2(Se_xS_{1-x})_6$.

Earlier the relationship between the optic and acoustic branches softening observed by neutron scattering and the incommensurate transition for the $Sn_2P_2Se_6$ crystal was considered in a simple model for the dispersion curves and interaction strengths, valid in the low-q continuum limit [9]. This model was suggested by the analysis of the spectra with the assumption of a real coupling between the optic and acoustic phonons. It was assumed that all of the soft fluctuation behaviour is contained in a 'bare' temperature dependent optic mode (polarization P_x), which interacts with a temperature independent acoustic mode (strain u_{xz}) via a temperature independent and real interaction strength. In this model a small change in the material parameters (an increase of the soft optic mode dispersion and acoustic phonons velocity or a decrease of their interaction parameter) will change the position of the instability from $q_i \neq 0$ to $q_i = 0$ [9].

3. Lattice dynamics in the polarizable ion model

3.1. Model description

To simulate the lattice instability of the PE phase of $Sn_2P_2S(Se)_6$ and to see what happens if one substitutes sulfur by selenium we calculate the spectra of order parameter fluctuations for several points near the LP in the T–x diagram of $Sn_2P_2(Se_xS_{1-x})_6$. Notice that the lattice dynamics calculations were performed previously in the framework of the rigid ion [25] and polarizable ion (polarizability of the sulfur atoms was included only) [26] model for $Sn_2P_2S_6$ only. But there has not been made any modelling of lattice instability in the PE phase of this crystal. We use the polarizable ion model (polarizability of all atoms is considered) [27]. The model parameters were defined by fitting the calculated phonon spectra to the data of Raman spectroscopy [28, 29], ultrasound investigations [17] and neutron scattering [9, 20]. The phonon spectra of $Sn_2P_2S(Se)_6$ were already analysed in [30].

An axial symmetry force field model [27] has been used to describe the short-range interactions. For the $Sn_2P_2S(Se)_6$ compounds the following short-range interactions have been taken into account: the internal anion interaction (between the first neighbours 'phosphorus–phosphorus', 'phosphorus–chalcogen', 'chalcogen–chalcogen' and between the second neighbours 'phosphorus–chalcogen') and the external interaction (between the first neighbours 'tin–chalcogen', 'tin–phosphorus', 'chalcogen–chalcogen'). The long-range part has been defined by effective charges and polarizabilities. The model contains 12 independent parameters: 7 radial force constants A_i for the short-range interaction, 5 for the long-range interaction (two effective charges and three polarizabilities). The tangential force constants have been determined from the static equilibrium conditions. The final set of parameters is given in table 3.

3.2. Low-frequency part of the phonon spectra in the PE phase

We shall now look in more detail at the lattice dynamics of the $Sn_2P_2S_6$ family in the PE phase. Let us consider the low-energy spectral part of the PE phase of $Sn_2P_2S_6$, $Sn_2P_2Se_6$ and their solid solutions. We concentrate on the lattice instability. Below the ferroelectric PT in $Sn_2P_2S_6$ ($P2_1/c \rightarrow Pc$) the transverse optical mode of B_u symmetry in the BZ centre condenses. The lowest calculated B_u symmetry optical mode is transverse and polarized in the symmetry plane

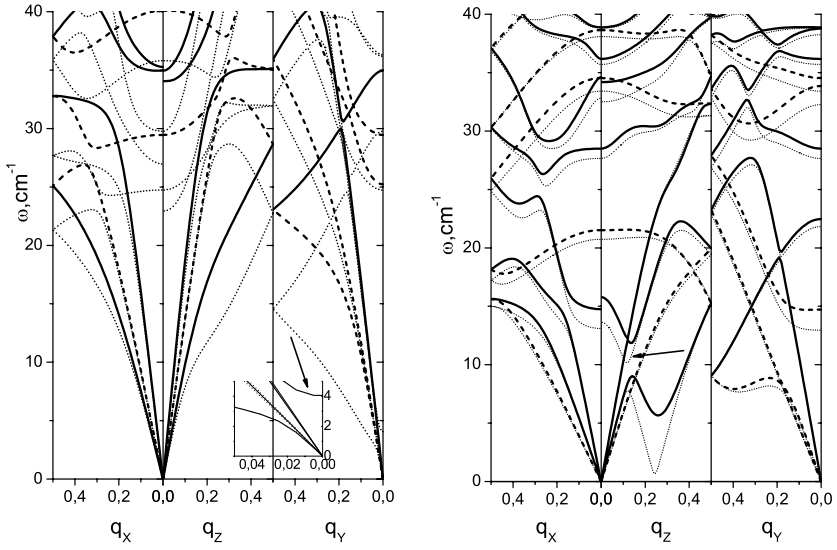

Figure 10. Different types of the modelled lattice instability (dotted lines versus continuous and dashed lines) in the PE phase of $Sn_2P_2S_6$ (left) and $Sn_2P_2Se_6$ (right) (the division in respect to symmetry: continuous lines—symmetry A′ modes for q_X and q_Z, and A for q_Y, dashed lines—symmetry A″ modes for q_X and q_Z, and B for q_Y; the arrows point to the soft optic mode location).

Table 3. Parameters of the polarizable ion model for $Sn_2P_2S_6$ and $Sn_2P_2Se_6$ in the FE and PE phases (short-range parameters are dimensionless quantities, effective charges in elementary charge units, polarizabilities in $Å^3$ units).

Force constant	$Sn_2P_2S_6$ FE	$Sn_2P_2S_6$ PE	$Sn_2P_2Se_6$ PE
A^0_{P-P}	215	216	177
A^0_{P-X} (near. neigb.)	283	248	227
A^0_{P-X} (next near. neigb.)	−6	1	4
A^0_{Sn-X}	27	15	27
A^0_{Sn-P}	−2	−3	−9
A^0_{X-X} (inter anion)	11	14	3
A^0_{X-X} (intra anion)	21	19	25
Z_{Sn}	1.2	1.45	0.91
Z_X	0.42	0.33	0.49
Z_P	0.54	0.59	0.47
α_{Sn}	1.5	3.3	4.5
α_X	2.8	1.1	1.7
α_P	0.6	1.3	0.05

close to the [100] direction. The dispersion curve of this mode has its minimum in the BZ centre (see figure 10). Though the interaction of this optical vibration with the acoustic ones is possible, no change in the dispersion curves of the latter has been observed.

The special feature of the calculated spectrum for $Sn_2P_2Se_6$ is a clearly defined minimum of the low-energy optical branch (with B_u symmetry in the BZ centre) below $q_Z \approx 0.15$ (see figure 10). The linear interaction of the mode with the transverse acoustic vibrations

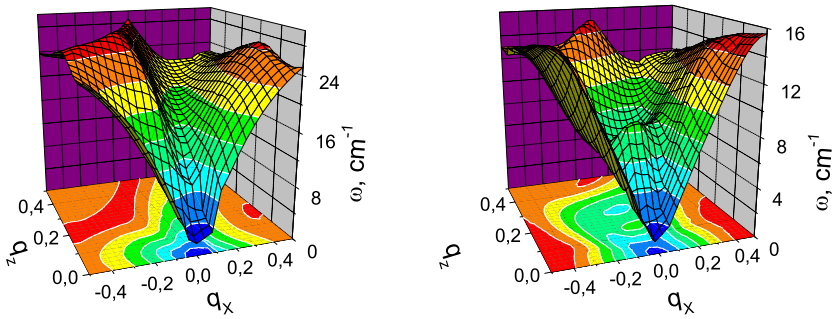

Figure 11. The energy surface, calculated in the symmetry plane, of the lowest acoustic vibration in the PE phase of $Sn_2P_2S_6$ (left) and $Sn_2P_2Se_6$ (right).

(This figure is in colour only in the electronic version)

having the same symmetry (A′), and polarized in the symmetry plane, preconditions a clear minimum in the acoustic branch below $q_Z \approx 0.25$. This situation agrees qualitatively with the experimentally observed pictures: in $Sn_2P_2Se_6$ a sequence of PTs of the second and the first order is seen on cooling. The transition from the high-temperature nonpolar phase to the polar one goes through a modulated incommensurate phase. The modulation period of this phase increases on cooling and is approximately 12–14 unit cells, which corresponds to the condensation of phonons at approximately $q \approx 0.1$ and the modulation vector is directed close to q_Z direction in the symmetry plane [8, 9].

So we find in the calculations of the lattice dynamics in the polarizable ion model an essential difference between $Sn_2P_2Se_6$ and $Sn_2P_2S_6$ in the dispersion curves of the transverse optical modes, connected with the PT and acoustic branches interacting with them.

3.3. Orientation dependence of the acoustic phonon branches

To check whether there are other minima in the phonon dispersion curves, in other directions, we have calculated the orientation dependence of the phonon spectra. In figure 11 the dispersion surface of the low-energy acoustic vibrations in the (010) reciprocal plane is given. As can be seen, there is a clearly marked difference between $Sn_2P_2Se_6$ and $Sn_2P_2S_6$: for the former there is a minimum in the direction close to q_Z (in agreement with the experiment in [9], the difference is about 9°), for the latter there is no minimum.

The calculations given for the acoustic surfaces make a comparison possible between the orientation dependence of the sound velocities obtained theoretically (see figure 12) and those obtained experimentally with Brillouin scattering (see figure 9). As can be seen, the polarizable ion model reflects qualitatively the anisotropy of the elastic properties of $Sn_2P_2S_6$. As long as Brillouin spectroscopy data are not available for $Sn_2P_2Se_6$, the same is not possible in that case, but we can compare the angular dependence of the sound velocities, experimentally investigated for $Sn_2P_2(Se_{0.28}S_{0.72})_6$ (see figure 9). As can be seen, the experimental orientation dependence of velocities of quasi-transverse acoustic phonons propagating and polarized in the monoclinic symmetry plane for both compositions ($x = 0$, $x = 0.28$) agree qualitatively with the calculated ones in the polarizable ion model from the dispersion surface of these phonons for $q \rightarrow 0$. However, in the experiment (see the temperature dependence of the transverse acoustic phonon velocity in figure 8 and the orientation dependence of this velocity in the PE phase near the PT temperature (see figure 9) for crystals with $x = 0.28$), no soft acoustic mode (i.e. the decrease of the transverse sound velocity for $q_i \rightarrow 0$ for $x \rightarrow x_{LP}$) has been observed,

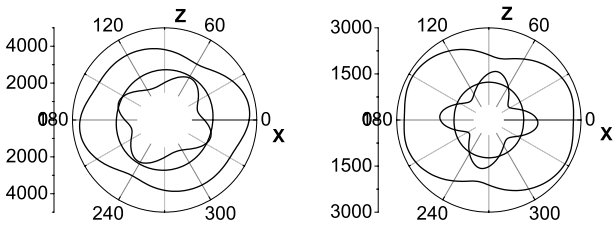

Figure 12. The indicatrix of the sound velocities in the PE phase calculated in the polarizable ion model for $Sn_2P_2S_6$ (left) and for $Sn_2P_2Se_6$ (right).

as would be expected for the LP in proper ferroelectrics. To clarify the possible reason for this absence of the acoustic mode softening in the PE phase of proper ferroelectrics under cooling to the LP (similar to the soft acoustic mode in proper ferroelastics), we modelled the PE phase lattice instability of the $Sn_2P_2S_6$ and $Sn_2P_2Se_6$ crystals with the following analysis of the instability, applied to the $Sn_2P_2(Se_xS_{1-x})_6$ solid solutions.

3.4. The lattice dynamical instability and the model parameters

We study here the dynamic instability in the polarizable ion model, varying its parameters. Because the displacement of the cation sublattice with respect to the anion one plays the main role in the PT, we vary the model parameters responsible for the interaction between the two sublattices. These are the radial force constant $A_{Sn-S/Se}$, the effective charges and the ion polarizabilities.

In the case of $Sn_2P_2S_6$ the change of the model parameters leads to the condensation of optical phonons in the BZ centre (figure 10). Notice that the optical mode softening takes place in the q_Y direction. This can be explained by the fact that the phonons with symmetry B_u (A′) propagating in the plane XOZ are skew (quasi-transverse or quasi-longitudinal) ones. This gives them an additional rigidity at the expense of the macroscopic field in comparison with the transverse B_u (B) phonons propagating in the q_Y direction.

The analysis of the data obtained confirms that the most important contribution to the lattice instability is the charge transfer between the tin and chalcogen atoms. Then the change of the ion charges causes in its turn a change of their polarizabilities; there is a unbalance of forces and the system becomes unstable for a well defined mode.

In $Sn_2P_2Se_6$ the change of the model parameters leads to the condensation of the mixed optic and acoustic phonons below $q_Z \approx 0.25$. While decreasing the A_{Sn-Se} constant, increasing the ion polarizability or changing the charge of the tin and selenium atoms the condensation of the interacting optical and acoustic phonons with small changes of other phonon branches (figure 10, dotted lines) happens.

To understand the reason for the difference between the PTs for $Sn_2P_2S_6$ and $Sn_2P_2Se_6$ we studied the influence of different interactions on the dispersion curves of the low-energy optic phonons. While taking into account only short range and Coulomb interaction in the rigid ion model, the frequencies of modes are increasing but the dispersion curves change to monotonically increasing curves with a minimum frequency value in the BZ centre (see figure 13). The instability modelling in this case shows that the phonons condense below $q_Y \rightarrow 0$ for both compounds. It is likely that at the expense of the macroscopic field the vibrations propagating in the q_Z direction have an additional hardness. The evident LO–TO splitting increases with the condensation of phonons, especially in $Sn_2P_2S_6$, which has higher values of the effective charges.

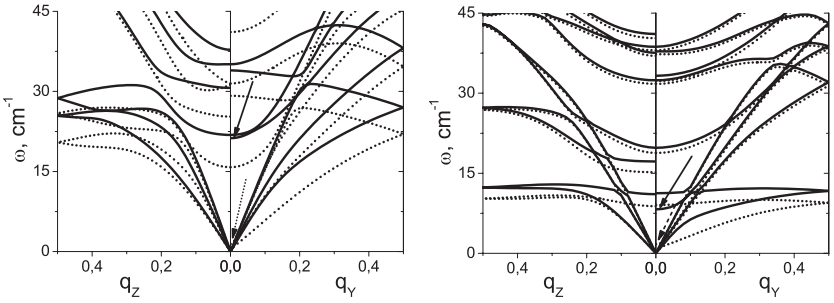

Figure 13. The phonon spectra of $Sn_2P_2S_6$ (left) and $Sn_2P_2Se_6$ (right) when only short range and Coulomb interactions are taken into account (in the rigid ion model). The solid lines correspond to the model parameters with the stable phonon spectra, the dotted ones to the modelled dynamic instability; the arrows point to the initial (stable) and final (unstable) location of the optic mode under destabilization.

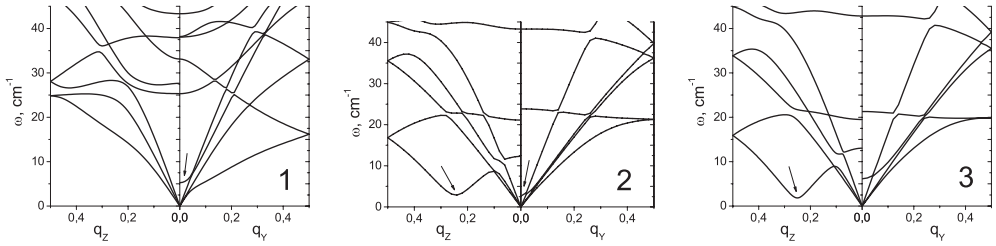

Figure 14. Different types of lattice instability modelled in $Sn_2P_2(Se_xS_{1-x})_6$ solid solution: $x = 0.25$—1, $x = 0.33$—2, $x = 0.4$—3; the arrows point to the points where phonon branches condense.

Including the polarizability of ions changes the situation drastically (figure 10). The frequency of the lowest optic B_u mode (under $q = 0$) decreases, but the dispersion curve now has a minimum near $q_Z \approx 0.25$ for the selenium, and at $q = 0$ for the sulfur compound. This modelling of the instability reproduces the experimental picture. Thus the ion polarizability is an important factor for the lattice dynamics and the instability in $Sn_2P_2S(Se)_6$. The change in the polarizability of ions and their charge state essentially influence the dispersion type of the soft optic mode of the crystals.

3.5. Solid solutions, the vicinity of the LP

To analyse the changes in the dispersion of the soft mode when substituting sulfur for selenium, the lattice dynamics of $Sn_2P_2(Se_xS_{1-x})_6$ was calculated within the framework of the so-called average crystal model. This model takes a linear approximation for the concentration dependence of all parameters which define the phonon spectrum. Of course, this model is very simplified. However, the similarity in the structure of the end member compounds, and the statistic character of chalcogen atom substitution in mixed crystals [31], let us expect a smooth behaviour of the concentration dependence of the phonon spectrum in the lower energy part.

We find (see figure 14) that for crystals with selenium concentration $0 < x < 0.33$ there is a condensation of optic phonons in the BZ centre. This is the case for $Sn_2P_2S_6$. For the solutions with $0.33 < x < 1$ there is condensation of mixed optic and acoustic phonons at $q_Z \approx 0.25$, similar to the case for $Sn_2P_2Se_6$. For the composition near $x \approx 0.33$ there is a

simultaneous condensation of phonons in the BZ centre and in another point of the BZ (see figure 14). This means that in our model there is a 'two-mode' concentration transformation for the spectrum of the order parameter fluctuations. It should be noted that the independence from the concentration of the wavevector of modulation ($q_Z \approx 0.25$) does not agree with the x-ray diffraction data given in [8], where they have obtained the behaviour $q^2 \sim (x - x_{\mathrm{LP}})$ expected for the LP case. However, it might be that it was impossible to separate experimentally the contributions from Bragg satellites approaching to the LP. Moreover, there are only data available for three values of the selenium concentration $x = 0.6, 0.8, 1.0$, and this does not allow one to determine accurately the concentration behaviour of the modulation wave vector in the IC phase near the LP. Obviously, it is desirable to carry out further investigations to define the concentration dependence of the wavevector of modulation of the IC phase in $Sn_2P_2(Se_xS_{1-x})_6$.

The relaxation component of the critical dynamics in $Sn_2P_2S(Se)_6$ [32] can, probably, also somewhat change the wavevector value at which the lattice instability of the PE phase occurs. However, the specific 'two-mode' concentration transformation of dispersion, as found in the polarizable ion model, agrees with the absence of the soft transverse acoustic mode in $Sn_2P_2(Se_{0.28}S_{0.72})_6$.

4. Conclusions

Brillouin spectroscopy has been carried out for the investigation of the temperature dependence of the acoustic properties in $Sn_2P_2(Se_xS_{1-x})_6$ at the PT, in the vicinity of the LP in the phase diagram. The sound velocity and attenuation anomalies at the ferroelectric second order PT are well described by the Landau–Khalatnikov theory. For increasing selenium concentration and approaching the LP ($x \approx 0.28$), the temperature interval where the hypersound velocity and attenuation deviate from its regular tendency in the PE phase grows, which is obviously caused by the enhancement of the order parameter fluctuations and the influence of structural defects on the critical anomalies. For the transverse acoustic phonons propagating in the (010) monoclinic plane near the [001] modulation direction in the IC phase and polarized in this plane close to the [100] spontaneous polarization direction, we have found a partial softening of the hypersound velocity under cooling to the PT temperature in the vicinity of the LP. This is a manifestation of a linear interaction of the soft optic mode dispersion branch with the transverse acoustic phonons branch near the BZ centre. This interaction is also manifest when we compare the group velocity surfaces in the PE phase of $Sn_2P_2S_6$ and $Sn_2P_2(Se_{0.28}S_{0.72})_6$ which were calculated on the basis of the Brillouin spectra for phonons propagating in different crystallographic directions. Lattice dynamics calculations of the compounds within the polarizable ion model were used for the study of the lattice instability of the proper uniaxial ferroelectrics in the vicinity of the LP. For $x < x_{\mathrm{LP}}$ at the PT from the PE phase to the FE phase the condensation of the soft optic mode having B_u symmetry has been modelled at $q_y \to 0$. For $x > x_{\mathrm{LP}}$ at the PT from the PE phase to the IC phase due to the strong enough $(\partial P_x/\partial z) \cdot u_{xz}$ interaction which corresponds to the Lifshitz invariant, the mixed optic and quasi-transverse acoustic phonons condense at $q_z > 0$. The fact that these mixed phonons have their propagation and polarization in the monoclinic symmetry plane explains the longitudinal component of the polarization for the soft optic mode, and preconditions consequently the additional hardness for the polarization fluctuations. This leads to an LO–TO splitting of the soft optic frequencies for phonons with $q_y \to 0$ and $q_z \to 0$. The larger effective charges in sulfur compounds is the reason for the increase of the LO–TO splitting when selenium is substituted for sulfur, and leads to the condensation of the soft optic mode at $q_y \to 0$ in the presence of a small $(\partial P_x/\partial y) \cdot u_{xy}$ interaction. In the vicinity of the LP the simultaneous

condensation of phonons has been modelled for $q_y \to 0$ and for $q_z > 0$. The mentioned 'two-mode' concentration transformation of the order parameter fluctuation spectrum is, obviously, a reason for the absence of the soft acoustic mode in Brillouin spectra, and a strong decrease of the velocity of transverse acoustic phonons in the PE phase, in the neighbourhood of the LP in $Sn_2P_2(Se_{0.28}S_{0.72})_6$.

Acknowledgments

One of us, R M Yevych, wishes to thank the staff of the Research Institute of Materials (University of Nijmegen) for their hospitality and assistance and Professor T Janssen for valuable advice in the phonon spectra calculations and interpretations. We are grateful to Professor T Janssen for the discussion of results and improving of this paper.

References

[1] Scott B, Pressprich M, Willet R and Cleary D 1992 *J. Solid State Chem.* **96** 294–300
[2] Dittmar G and Schafer H 1974 *Z. Naturf.* b **29** 312–7
[3] Yamada Y, Fujii Y and Hatta J 1968 *J. Phys. Soc. Japan* **24** 1053–8
[4] Ishibashi Y and Shiba H 1978 *J. Phys. Soc. Japan* **45** 409–13
[5] Vysochanskii Yu and Slivka V 1992 *Sov. Phys.—Usp.* **35** 123–34
[6] Vysochanskii Yu *et al* 1989 *JETF* **45** 1355–65
Khoma M, Molnar A and Vysochanskii Yu 1998 *J. Phys. Studies* **2** 524–35
[7] Hornreich R, Luban M and Shtrikman S 1975 *Phys. Rev. Lett.* **35** 1678–81
[8] Barsamian T, Khasanov S and Shekhman V 1993 *Ferroelectrics* **138** 63–77
[9] Eijt S, Currat R, Lorenzo E, Saint-Gregoire P, Katano S, Janssen T, Hennion B and Vysochanskii Yu 1998 *J. Phys.: Condens. Matter* **10** 4811–44
[10] Major M, Vysochanskii Yu and Pritz I 1990 *Kristallografija* **35** 1300–2
[11] Folk R and Moser G 1993 *Phys. Rev.* B **47** 13992–7
Folk R 1999 *Phase Transit.* **67** 645–66
[12] Molnar A, Vysochanskii Yu, Horvat A and Nakonechnii Yu 1997 *Ferroelectrics* **192** 137–48
[13] Samulionis V, Banys J and Vysochanskii Yu 1999 *Phys. Status Solidi* b **215** 1151–6
[14] Vysochanskii Yu, Mitrovcij V, Grabar A, Perechinskii S, Motrija S and Kroupa J 2000 *Ferroelectrics* **237** 193–200
[15] Hlinka J, Currat R, de Boissieu M, Livet F and Vysochanskii Yu 2005 *Phys. Rev.* B **71** 2102–5
[16] Levanyuk A and Sannikov D 1976 *Fiz. Tverd. Tela* **18** 1927–32
[17] Valyavichus V, Samulionis V and Vysochanskii Yu 1989 *Fiz. Tverd. Tela* **31** 144–8
[18] Vysochanskii Yu *et al* 1984 *Fiz. Tverd. Tela* **26** 3469–72
[19] Yevych R M, Perechinskii S I, Grabar A A and Vysochanskii Yu M 2004 *Ferroelectrics* **298** 97–101
[20] Eijt S, Currat R, Lorenzo J, Saint-Gregoire P, Hennion B and Vysochanskii Yu 1998 *Eur. Phys. J.* B **5** 169–78
[21] Vysochanskii Yu, Mayor M, Perechinsky S and Tihomirova N 1992 *Kristallografija* **37** 171–6
[22] Bruce A D and Cowley R A 1981 *Structural Phase Transitions* (London: Taylor and Francis)
[23] Landau L D and Khalatnikov I M 1954 *Dokl. SSSR* **96** 469–72
[24] Maior M, Gurzan M, Molnar Sh, Prits I and Vysochanskii Yu 2000 *Trans. Ultrason. Ferroelectr. Frequency Control* **47** 877–80
[25] Grabar A A, Yevych R M and Vysochanskii Yu M 2000 *Kristallografija* **45** 876–80
[26] Smirnov M B, Hlinka J and Solov'ev A V 2000 *Phys. Rev.* B **61** 15051–9
[27] Born M and Huang K 1954 *Dynamical Theory of Crystal Lattices* (Oxford: Oxford University Press)
Bruesch P 1982 *Phonons: Theory and Experiments. I. Lattice Dynamics and Models of Interatomic Forces* (Berlin: Springer) p 261
[28] Bokotei A, Vysochanskii Yu, Rizak V, Stefanovich V and Gurzan M 1997 *Ukr. Fiz. J.* **42** 55–62
Vysochanskii Yu, Slivka V, Voroshilov Yu, Gurzan M and Chepur D 1979 *Fiz. Tverd. Tela* **21** 211–5
[29] Hlinka J *et al* 2002 *Phys. Rev.* B **65** 1–9
[30] Yevych R and Vysochanskii Yu 2006 *Condens. Matter Phys.* at press
[31] Vysochanskii Yu, Stefanovich V, Mytrovcij V, Mykajlo O, Yevych R and Gurzan M 2002 *Ferroelectrics* **267** 397–402
[32] Vysochanskii Yu and Drobnich A 2002 *Condens. Matter Phys.* **5** 669–83